

STM3: Mixture of Multiscale Mamba for Long-Term Spatio-Temporal Time-Series Prediction

Haolong Chen

Shenzhen Research Institute of Big Data
Shenzhen, Guangdong, China
The Chinese University of Hongkong, Shenzhen
Shenzhen, Guangdong, China
haolongchen1@link.cuhk.edu.cn

Zhengyuan Xin

Shenzhen Research Institute of Big Data
Shenzhen, Guangdong, China
The Chinese University of Hongkong, Shenzhen
Shenzhen, Guangdong, China
zhengyuanxin@link.cuhk.edu.cn

Liang Zhang*

School of Cyber Science and Technology, Shenzhen
Campus of Sun Yat-sen University
Shenzhen, Guangdong, China
zhangliang27@mail.sysu.edu.cn

Guangxu Zhu*

Shenzhen Research Institute of Big Data
Shenzhen, Guangdong, China
The Chinese University of Hongkong, Shenzhen
Shenzhen, Guangdong, China
gxzhu@sribd.cn

Abstract

Recently, spatio-temporal time-series prediction has developed rapidly, yet existing deep learning methods struggle with learning complex long-term spatio-temporal dependencies efficiently. The long-term spatio-temporal dependency learning brings two new challenges: 1) The long-term temporal sequence includes multi-scale information naturally which is hard to extract efficiently; 2) The multiscale temporal information from different nodes is highly correlated and hard to model. To address these challenges, we propose an efficient *Spatio-Temporal Multiscale Mamba* (STM2) that includes a multiscale Mamba architecture to capture the multiscale information efficiently and simultaneously, and an adaptive graph causal convolution network to learn the complex multiscale spatio-temporal dependency. STM2 includes hierarchical information aggregation for different-scale information that guarantees their distinguishability. To capture diverse temporal dynamics across all spatial nodes more efficiently, we further propose an enhanced version termed *Spatio-Temporal Mixture of Multiscale Mamba* (STM3) that employs a special Mixture-of-Experts architecture, including a more stable routing strategy and a causal contrastive learning strategy to enhance the scale distinguishability. We prove that STM3 has much better routing smoothness and guarantees the pattern disentanglement for each expert successfully. Extensive experiments on real-world benchmarks demonstrate STM2/STM3's superior performance, achieving state-of-the-art results in long-term spatio-temporal time-series prediction.

*Liang Zhang and Guangxu Zhu are corresponding authors.

Permission to make digital or hard copies of all or part of this work for personal or classroom use is granted without fee provided that copies are not made or distributed for profit or commercial advantage and that copies bear this notice and the full citation on the first page. Copyrights for components of this work owned by others than the author(s) must be honored. Abstracting with credit is permitted. To copy otherwise, or republish, to post on servers or to redistribute to lists, requires prior specific permission and/or a fee. Request permissions from permissions@acm.org.
Conference acronym 'XX, Woodstock, NY

© 2018 Copyright held by the owner/author(s). Publication rights licensed to ACM.
ACM ISBN 978-1-4503-XXXX-X/2018/06
<https://doi.org/XXXXXXX.XXXXXXX>

CCS Concepts

• Computing methodologies → Neural networks.

Keywords

Spatio-Temporal Time-Series Prediction, Mixture-of-Experts, Selective State Spaces

ACM Reference Format:

Haolong Chen, Liang Zhang, Zhengyuan Xin, and Guangxu Zhu. 2018. STM3: Mixture of Multiscale Mamba for Long-Term Spatio-Temporal Time-Series Prediction. In *Proceedings of Make sure to enter the correct conference title from your rights confirmation email (Conference acronym 'XX)*. ACM, New York, NY, USA, 14 pages. <https://doi.org/XXXXXXX.XXXXXXX>

1 Introduction

Spatio-temporal time-series prediction is fundamental to applications like traffic forecasting and environmental monitoring, where modeling both temporal dynamics and spatial dependencies across multiple time series is essential. While deep learning methods like RNNs, CNNs, GNNs, and Transformers etc., have achieved remarkable success in this domain [2, 18, 25, 27, 28, 39, 44, 48, 48, 52], existing approaches still face limitations in long-term spatio-temporal modeling. Specifically, performance degrades significantly as the prediction horizon increases, primarily due to insufficient modeling of information flow mechanisms during feature fusion across complex long-term spatio-temporal patterns.

Recently, State Space Models (SSMs) have re-emerged as a powerful framework for capturing long-range dependencies [12, 17, 32, 38], with innovations like Mamba [16] introducing time-varying parameters and hardware-aware parallelization to significantly improve efficiency. While preliminary attempts have applied SSMs to long-term spatio-temporal data [10, 24], these approaches typically capture dependencies similarly to short-term data and thus fail to address the intertwined nature of long-term dynamics, as seen in STG-Mamba [24], which incorporates local spatial adjacency but neglects comprehensive spatio-temporal interactions. Modeling long-term spatio-temporal dependencies introduces two new challenges. 1) Long-term sequences inherently contain multiscale

information. For instance, minute-level traffic data captures immediate patterns, whereas hour-level data reflects daily periodicities like rush hours. Although SSMs effectively capture fine-grained temporal dependencies, they struggle to simultaneously learn multiscale patterns. 2) The multiscale temporal information across spatial nodes is highly correlated yet heterogeneous, complicating the modeling process. For example, traffic flow patterns differ significantly between highways and central business districts. The challenge lies in effectively modeling these complex interactions between spatial information and multiscale temporal patterns, which have not been fully explored.

To address these challenges, we propose *Spatio-Temporal Multiscale Mamba* (STM2), an efficient architecture combining two key components: 1) a multiscale Mamba for multiscale temporal pattern extraction; 2) an adaptive graph causal convolution network (AGCCN) for modeling long-term spatio-temporal dependencies. Regarding the first challenge, while multiscale feature extraction has shown promise in prior work [7, 14, 18, 35, 44, 50], existing approaches suffer from substantial computational overhead when processing multiscale long-term sequences. Our multiscale Mamba overcomes this by efficiently reusing channels within a single Mamba block, augmented with learnable scale-specific biases, thus maintaining Mamba’s computational advantages. For the second challenge, each node needs to aggregate information selectively from the most relevant neighboring nodes and corresponding scales. Our proposed AGCCN introduces two innovations: it learns an adaptive graph structure shared across temporal scales while employing causal attention to identify critical cross-scale interactions. This design ensures hierarchical information flow - each node aggregates features from relevant neighbors at the same or coarser scales while avoiding interference from finer scales, thereby preserving scale distinguishability and modeling complex spatio-temporal relationships.

As spatio-temporal dependencies become increasingly complex, relying solely on a single multiscale Mamba in STM2 becomes insufficient for capturing diverse temporal dynamics across different nodes, especially given heterogeneous multiscale patterns from different spatial nodes. To overcome this limitation, we adopt a Mixture-of-Experts (MoE) architecture [19] and propose an enhanced framework termed *Spatio-Temporal Mixture of Multiscale Mamba* (STM3). STM3 employs multiple expert models to partition and handle intricate data distributions, with each data subset processed by only a small number of experts. This approach significantly improves representational capacity while maintaining manageable computational complexity. Unlike previous MoE approaches [1, 37, 46], we leverage static node embeddings learned from the adaptive network rather than dynamic input features as gating inputs, resulting in significantly improved routing smoothness. Additionally, to further enhance the distinguishability of scale information across experts, we introduce a novel causal contrastive learning method that explicitly considers directional similarity, thus guaranteeing successful disentanglement of patterns for each expert.

In summary, we have made the following contributions: 1) We introduce STM2, a novel and effective framework specifically designed for modeling complex long-term spatio-temporal dependencies, featuring a multiscale Mamba architecture for multiscale

temporal information capturing and an adaptive graph causal convolution network for intricate spatio-temporal dependency modeling. 2) We propose an enhanced framework, STM3, utilizing a specialized Mixture-of-Experts architecture to better capture diverse temporal dynamics across spatial nodes. We prove that STM3 has significant improvements in routing smoothness and guarantees the pattern disentanglement for each expert. 3) Comprehensive experiments on large-scale real-world datasets demonstrate that STM3 achieves state-of-the-art performance.

2 Related Work

Spatio-Temporal Time-Series Prediction. Recent years have witnessed remarkable progress in spatio-temporal time-series prediction, driven by advances in deep neural networks specifically designed to capture complex spatial and temporal dependencies. For temporal pattern modeling, researchers have leveraged diverse architectures, including RNNs [2, 27, 52], CNNs [44, 48], and attention mechanisms [18, 28]. The recent emergence of Mamba-based approaches has introduced promising new directions in spatial correlation modeling [10, 22, 24, 49]. Grounded in the theoretical foundations of SSMs, these methods demonstrate exceptional efficiency in processing sequential data. On the spatial modeling front, GNNs have become prevalent in capturing inter-region dependencies via graph-structured message passing [25, 39, 48]. Pioneering works such as DCRNN [25] and STGCN [48] employed predefined graph structures for spatial relationships, and subsequent developments introduced adaptive graph learning methods—including Graph Wavenet [45], MTGNN [44], and AGCRN [2]—which dynamically infer graph structures from data. Further architecture improvements were attained through Neural ODE-based approaches [9] and self-supervised learning techniques [26]. In this work, we extend Mamba [16] to construct a Multiscale Mamba architecture for spatio-temporal modeling. Our proposed approach also integrates adaptive graph causal convolution and a special MoE architecture, jointly capturing multiscale temporal dynamics and spatial dependencies.

More related work for State Space Models and Mixture-of-Experts is summarized in the Appendix A.

3 Problem Definition

Spatio-Temporal Data. Spatio-temporal data refer to data points collected from the real world within a specific region and time period. We represent it as a tensor $X = [x_0, x_1, \dots, x_t, \dots]$, where each $x_t \in \mathbb{R}^{N \times C}$ denotes the recorded C features of N nodes at time step t .

Spatial Graph. We consider a spatial graph $\mathcal{G} = (\mathcal{V}, \mathcal{E}, \mathcal{A})$ to capture spatial relationships among nodes, where \mathcal{V} is the set of N nodes, \mathcal{E} represents the set of edges, and \mathcal{A} denotes the adjacency matrix of the graph, capturing proximity between nodes.

Spatio-Temporal Time-Series Prediction. Spatio-temporal time-series prediction involves forecasting future spatio-temporal series based on historical observations. Given the historical data $X \in \mathbb{R}^{T \times N \times C}$, the goal of spatio-temporal time-series prediction is to estimate future data $Y \in \mathbb{R}^{\tau \times N \times C}$, where T denotes the number of historical input timesteps and τ represents the prediction horizon.

4 Methodology

4.1 Model Architecture

In this section, we present the main architecture of STM3, an effective solution for long-term spatio-temporal time-series prediction, as illustrated in Figure 1. The model comprises three primary components: a multiscale feature extraction module for decomposing multiscale features, an Adaptive Graph Causal Convolution Network (AGCCN) module for aggregating multiscale spatio-temporal information, and a Mixture of Multiscale Mamba (MMM) module that employs multiple multiscale Mamba experts to capture diverse long-term temporal patterns. Below, we provide a detailed description of each component to facilitate a deeper understanding of the architecture.

4.2 Multiscale Preprocessing

We first introduce the multiscale preprocessing step, which provides a basic representation of multiscale series. Specifically, we employ a linear layer as the input head to project the input $X \in \mathbb{R}^{T \times N \times C}$ into raw features $H \in \mathbb{R}^{T \times N \times d}$. Subsequently, the multiscale preprocessing module decomposes these raw features H using multiple 1-dimensional temporal convolution layers with varying kernel sizes, formulated as follows:

$$H_{\text{ms}}^{(q)} = \text{Conv1d}(H, s_0^{(q)}), \quad \forall q \in [1, Q], \quad (1)$$

where $H_{\text{ms}}^{(q)} \in \mathbb{R}^{T \times N \times d}$ denotes the feature representation at the initial scale $s_0^{(q)} \in \mathbb{Z}^+$. We define scales such that $s_0^{(i)} \leq s_0^{(j)}$ when $i \leq j$, ensuring that the information at different scales is arranged progressively from fine to coarse granularity. Here, $\text{Conv1d}(\cdot, s)$ indicates a 1-dimensional temporal convolution with kernel size s . Finally, we stack all the features after convolution as the final output $H_{\text{ms}} \in \mathbb{R}^{T \times N \times d \times Q}$.

4.3 Adaptive Graph Causal Convolution Network

Adaptive Graph Causal Convolution Network (AGCCN) attempts to learn the complex correlation between the multiscale temporal information and the spatial information. There exist two challenges. 1) The high computational complexity. If we analyze the connection of all nodes among all scales, we need at least the time complexity $O(N^2 Q^2 T d)$, which is unacceptable when the problem becomes large enough. 2) The unknown hidden spatial relationship. It would be hard to obtain from the real graph, such as the distance graph. To address them, we propose an adaptive causal convolution network with a learnable graph shared across all scales. Spatial information is first aggregated based on this graph, followed by causal attention for hierarchical information aggregation. At the same time, the total time complexity is reduced to $O(N Q^2 T d)$.

We maintain a learnable node embedding dictionary $E_A \in \mathbb{R}^{N \times d_e}$ for all nodes, where each row of E_A represents the embedding of a node and d_e denotes the dimension of node embedding. Then, we can yield the normalized Laplacian directly:

$$D^{-1/2} A D^{-1/2} = \text{softmax}(\text{ReLU}(E_A E_A^\top)) \quad (2)$$

where $A \in \mathbb{R}^{N \times N}$ is the adjacent matrix, and D is the degree matrix. This allows joint graph structure learning with prediction objectives, overcoming domain-specific heuristic limitations.

Let $H_{\text{in}} \in \mathbb{R}^{N \times d \times Q}$ where Q denotes the number of temporal scales denote the input traffic of a specific time step t , here we omit the subscript t for brevity, and the 1st order Chebyshev polynomial expansion approximated GCN operation follows:

$$H_G^{(q)} = (I_N + D^{-1/2} A D^{-1/2}) H_{\text{in}}^{(q)} \Theta + b, \quad (3)$$

$$\Theta = E_g W_g, \quad b = E_g b_g, \quad \forall q \in [1, Q],$$

where $I_N \in \mathbb{R}^{N \times N}$ is identity matrix, $\Theta \in \mathbb{R}^{N \times d \times d}$, $b \in \mathbb{R}^{N \times d}$ are learnable parameters, and $H_G \in \mathbb{R}^{N \times d \times Q}$ is the output of the adaptive graph convolution. For better optimization of the huge parameter matrices Θ and b , a low-rank adaptation approach is introduced as $\Theta = E_g W_g$, $b = E_g b_g$, where $d_{\text{low}} \ll N$, $E_g \in \mathbb{R}^{N \times d_{\text{low}}}$, $W_g \in \mathbb{R}^{d_{\text{low}} \times d \times d}$, $b_g \in \mathbb{R}^{d_{\text{low}} \times d}$ are learnable parameters.

After aggregating spatial information, H_{GCN} is processed by causal attention to aggregate cross-scale information. The mechanism ensures hierarchical information aggregation, i.e., fine-grained features selectively retrieve coarser-grained information while preventing redundant reverse processes, thus avoiding information entanglement. The causal attention mechanism is as follows:

$$Q = \text{Linear}_Q(H_G^\top), \mathcal{K} = \text{Linear}_K(H_G^\top), \mathcal{V} = \text{Linear}_V(H_G^\top), \quad (4)$$

$$H_{\text{atten}} = \text{softmax}\left(\frac{Q K^\top}{\sqrt{d}} + \mathcal{M}\right) V, \quad \text{where} \quad (5)$$

$$\mathcal{M}^{(i,j)} = \begin{cases} 0 & \text{if } i \geq j \\ -\infty & \text{otherwise} \end{cases},$$

$$H_{\text{out}} = \text{LayerNorm}(\text{Linear}_{\text{out}}(H_{\text{atten}})^\top + H_G), \quad (6)$$

where Linear_Q , Linear_K , Linear_V and $\text{Linear}_{\text{out}}$ project the feature into the corresponding space. The lower-triangle causal attention mask $\mathcal{M} \in \mathbb{R}^{Q \times Q}$ constrains the rule “only coarse-grained information can flow towards fine-grained information”. Finally, the feature after attention is projected to the output space, added with the residual input H_{GCN} , and normalized as the output feature H_{out} .

4.4 Multiscale Mamba

Although the standard Mamba architecture effectively models long-term dependencies, it exhibits inherent limitations in simultaneously capturing multiscale temporal patterns. To address this, we propose a novel Multiscale Mamba module. Let $H_{\text{in}} \in \mathbb{R}^{T \times d \times Q}$ denote the input feature under a specific spatial node n . Here we omit the subscript n for brevity. After input projection, we can get the Mamba’s latent feature $h_{\text{ms}} = \text{Linear}(H_{\text{in}})$.

Scale Amplification. In the previous multiscale preprocessing module, a single input sequence is transformed into multiple sequences at Q different temporal scales. Modeling long-term dependencies typically requires a large number of scale levels, which can incur high computational costs. To address this, we introduce a scale amplification mechanism that enables Mamba to capture additional temporal scales with low overhead. Structurally similar to multiscale preprocessing, it applies 1D temporal convolutions for scale amplification as follows:

$$h^{(q)} = \text{Conv1d}(h_{\text{ms}}^{(q)}, s^{(q)}), \quad \forall q \in [1, Q], \quad (7)$$

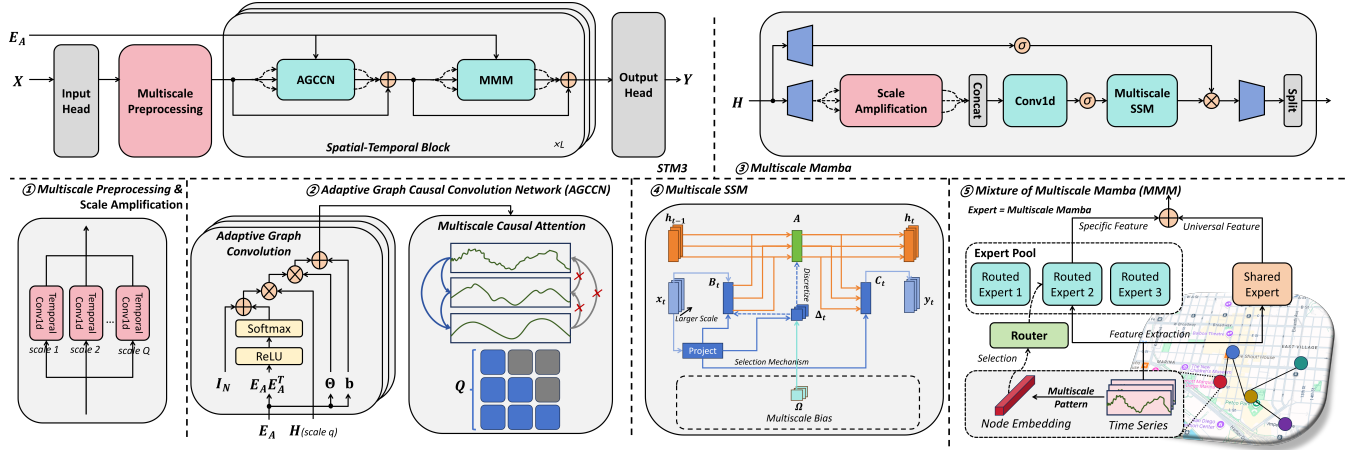


Figure 1: Main structure of STM3.

where $h_{ms}^{(q)} \in \mathbb{R}^{T \times d_{inner}}$ and $h^{(q)} \in \mathbb{R}^{T \times d_{inner}}$ denote the input and output feature sequences at scale q . We then stack the outputs to obtain $h \in \mathbb{R}^{T \times d_{inner} \times Q}$, with symbols consistent with Section 4.2. Through scale amplification, the maximum scale expands to $s_0^{(Q)} [s^{(Q)}]^L$, where L denotes the layer index of the backbone where the multiscale Mamba module is deployed, enabling an exponentially growing temporal receptive field.

Multiscale SSM. The standard Mamba SSM uses a data-dependent selection mechanism to generate its parameters, which is inadequate for capturing distinct autocorrelation patterns across scales. Using separate SSMs per scale increases parameter count linearly and fails to model cross-scale interactions, while sharing a single SSM causes information entanglement and degrades performance. To address this trade-off, we propose a novel multiscale SSM module that enables simultaneous multiscale pattern extraction.

We first concatenate temporal features from different scales along the feature dimension to form $\hat{h} \in \mathbb{R}^{T \times (Q \cdot d)}$, then project it to form the input-aware parameters as follows:

$$[\Delta, B, C] = \tanh(W_{proj}(\hat{h})). \quad (8)$$

The input-aware parameters are learned across all scales, enabling a comprehensive understanding of the series. However, sharing them across all sequences ignores scale-specific differences. To address this, the multiscale SSM introduces a learnable bias term $\Omega \in \mathbb{R}^{(Q \cdot d)}$ added to Δ , guiding the SSM to perform scale-specific pattern extraction. This modified Δ enables precise control over the SSM's behavior by adjusting the discretization of matrices A and B . The scale-specific and input-aware parameters are then updated as:

$$\hat{\Delta} = \text{Linear}(\Delta) + \text{broadcast}(\Omega), \quad \tilde{A} = \exp(\hat{\Delta} \otimes A), \quad \tilde{B} = \hat{\Delta} \otimes B. \quad (9)$$

Based on the above parameters, the SSM function is introduced as:

$$u^{(t)} = \tilde{A}u^{(t-1)} + \tilde{B}\hat{h}^{(t)}, \quad h_{final}^{(t)} = Cu^{(t)}. \quad (10)$$

By integrating the scale amplification module with the multiscale SSM, we propose Multiscale Mamba that effectively captures temporal dependencies at multiple time scales. The full computational procedure is detailed in Algorithm 1.

Algorithm 1 Multiscale Mamba

Require: Input sequence $H_{in} \in \mathbb{R}^{T \times d \times Q}$, scales $\mathcal{S} = [s_1, \dots, s_Q] \in \mathbb{R}^Q$

Ensure: Output sequence $H_{out} \in \mathbb{R}^{T \times d \times Q}$

1. Input Projection

$$\hat{H}_{in} \leftarrow \text{Concat}(H_{in}), \hat{H}_{in} \in \mathbb{R}^{T \times (d \cdot Q)}$$

$$[h, z] \leftarrow \text{Linear}(\hat{H}_{in}), h \in \mathbb{R}^{T \times (d_{inner} \cdot Q)}, z \in \mathbb{R}^{T \times (d_{inner} \cdot Q)}$$

2. Multiscale Feature Extraction

$$h_{ms} = \text{reshape}(h) \in \mathbb{R}^{T \times d_{inner} \times Q}$$

for $q \leftarrow 1$ **to** Q **do**

$$h^{(q)} \leftarrow \text{Conv1D}(h_{ms}^{(q)}, s_q)$$

end for

$$\hat{h} \leftarrow \text{concat}(h^{(1)}, \dots, h^{(Q)}), \hat{h} \in \mathbb{R}^{T \times (d_{inner} \cdot Q)}$$

3. Global Temporal Mixing

$$\hat{h} \leftarrow \text{SiLU}(\text{CausalConv1D}(\hat{h}))$$

4. Selection Mechanism With Multiscale Bias

$$[\Delta, B, C] \leftarrow \tanh(W_{proj}(\hat{h}))$$

$$\hat{\Delta} \leftarrow \text{Linear}(\Delta) + \text{broadcast}(\Omega), \hat{\Delta} \in \mathbb{R}^{T \times (d_{inner} \cdot Q)}, \Omega \in \mathbb{R}^{(d_{inner} \cdot Q)}$$

5. Discretization

$$\tilde{A} \leftarrow \exp(\hat{\Delta} \otimes A)$$

$$\tilde{B} \leftarrow \hat{\Delta} \otimes B$$

6. Parallel Selective Scan

$$h_{final} \leftarrow \text{SSM}(\tilde{A}, \tilde{B}, C, \hat{h}), h_{final} \in \mathbb{R}^{T \times (d_{inner} \cdot Q)}$$

7. Gated Output

$$h_{out} \leftarrow \text{SiLU}(z) \odot h_{final}, h_{out} \in \mathbb{R}^{T \times (d_{inner} \cdot Q)}$$

$$\hat{H}_{out} \leftarrow \text{Linear}(h_{out}), \hat{H}_{out} \in \mathbb{R}^{T \times (d \cdot Q)}$$

$$H_{out} \leftarrow \text{Split}(\hat{H}_{out})$$

return H_{out}

4.5 Mixture of Multiscale Mamba

In previous subsections, we introduced multiscale Mamba for efficient multiscale information extraction and AGCCN for learning complex multiscale spatial-temporal correlations, which together

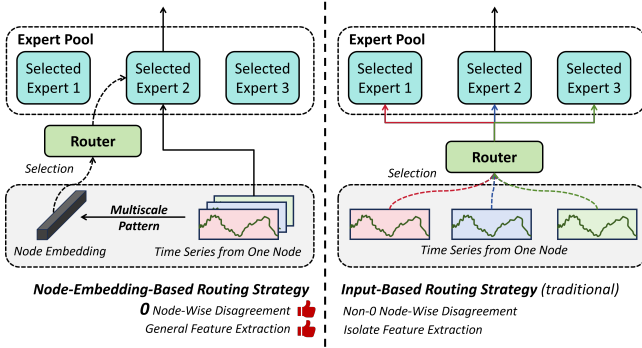


Figure 2: The comparison between two routing strategies.

form STM2. However, a single Multiscale Mamba in STM2 struggles to capture diverse temporal dynamics when spatial-temporal dependencies grow more complex. To address this, we propose a Mixture of Multiscale Mamba (MMM), an MoE variant of multiscale Mamba, to form STM3.

Experts. In the MMM layer, we implement two types of experts: (1) a persistent multiscale Mamba serving as shared expert E_0 that processes all input data to capture universal temporal patterns, and (2) K independent multiscale Mamba with distinct parameterizations as specialized experts $\{E_k\}_{k=1}^K$ that capture specific temporal patterns. Each expert $E_k(\cdot) : \mathbb{R}^{T \times d \times Q} \rightarrow \mathbb{R}^{T \times d \times Q}$, $k \in [0, K]$ learns different temporal dynamics through its state transition mechanism. Since temporal sequences typically contain both shared and unique multiscale patterns, the shared expert E_0 extracts common features while the specialized experts $\{E_k\}_{k=1}^K$ focus on distinctive temporal characteristics. Note that we select only one specialized expert for each input.

Routing Strategy. We propose a novel **node-embedding-based routing strategy** to determine the appropriate specialized expert. Unlike traditional approaches that directly use input series for gating decisions, we employ the learnable node embeddings E_A introduced in Section 4.3. These embeddings serve as node identifiers and provide more stable routing patterns. Formally, we define the gating network as $G(\cdot) : \mathbb{R}^{d_e} \rightarrow \mathbb{R}^K$, implemented as a bias-free linear layer with added random noise to improve routing robustness [8]. For an input time series $x_{in} \in \mathbb{R}^{T \times d \times Q}$ of a node with corresponding learnable embedding $e_{in} \in \mathbb{R}^{d_e}$ capturing its intrinsic characteristics, the MMM output $z \in \mathbb{R}^{T \times d \times Q}$ is computed as:

$$z = \sum_{k=1}^K \mathbb{I}[i = g] E_k(x_{in}) + E_0(x_{in}), \quad g = \operatorname{argmax}_{k \in [K]} \{G_k(e_{in}) + r_k\}, \quad (11)$$

where g denotes the top-1 selection of the expert, G_k denotes the gating network's output for expert k , r denotes a random noise $r \sim \mathcal{U}(0, b_{up})$. We compare the traditional input-based routing strategy and our proposed node-embedding-based routing strategy in Figure 2. Additionally, we prove that our method exhibits smoother behavior by the following lemma.

LEMMA 1. Let $\mathbf{H} = [\mathbf{h}_1, \mathbf{h}_2, \dots, \mathbf{h}_M] \in \mathbb{R}^{M \times K}$ be the set of the gating network's output of M samples, which belongs to one spatial node and $\mathbf{r} = [r_1, r_2, \dots, r_K] \in \mathbb{R}^K$ be independent noise vectors drawn

from \mathcal{D}_r with ρ -bounded probability density function. Define the pairwise routing disagreement probability $p_{i,j}$ and the node-wise disagreement probability \mathbf{P} as follows:

$$p_{i,j} = \mathbb{P}(\operatorname{argmax}_{k \in [K]} \{h_{i,k} + r_k\} \neq \operatorname{argmax}_{k \in [K]} \{h_{j,k} + r_k\}). \quad (12)$$

$$\mathbf{P} = \mathbb{P}(\exists i \neq j \in [M], \text{ s.t. } \operatorname{argmax}_{k \in [K]} \{h_{i,k} + r_k\} \neq \operatorname{argmax}_{k \in [K]} \{h_{j,k} + r_k\}). \quad (13)$$

Then it satisfies:

$$0 \leq \mathbf{P} \leq \rho K^2 \sum_{i < j} \|\mathbf{h}_i - \mathbf{h}_j\|_\infty, \quad (14)$$

and for our node-embedding-based routing, $\mathbf{P} \equiv 0$.

Lemma 1 proves that our node-embedding-based routing achieves $\mathbf{P} \equiv 0$, satisfying our key design principle: sequence samples from the same spatial nodes share identical transition patterns, and ensuring smooth routing. In contrast, conventional input-based routing always produces non-zero \mathbf{P} , resulting in routing unsmoothness. The complete proof is provided in Appendix B.1.

Loss Design. With the STM3, we can use the sequences before time t to learn the prediction for the future τ step data, denoted as $\{\tilde{x}_{t+i}\}_{i=1}^\tau$. Then, we have the following loss:

$$\mathcal{L}_{MAE} = \mathbb{E}_{i=1}^\tau \|\tilde{x}_{t+i} - x_{t+i}\|_2^2. \quad (15)$$

Directly optimizing \mathcal{L}_{MAE} to learn from specialized experts may lead to unstable training. If the gating network fails to provide stable routing, each expert may extract similar information.

To encourage experts to learn distinct content, contrastive learning offers an intuitive solution: treating outputs from the same expert as positive samples and those from different experts as negative samples. However, it assumes correct routing during training. In practice, we cannot guarantee that two samples routed to the same expert are truly similar when routing errors occur. Thus, the challenge lies in identifying reliable positive samples.

Fortunately, our analysis shows that coarser-scale outputs within a sample can effectively serve as positive samples for learning higher-level features, while finer-scale outputs should be treated as negatives to preserve scale distinguishability. This leads to an asymmetric similarity measure where $s(x, x') \neq s(x', x)$. Traditional contrastive learning relies on symmetric metrics (e.g., cosine similarity), which are unsuitable in this context. To address this, we propose a novel **causal contrastive learning** method. First, we define an asymmetric causal measurement: for two outputs $(x_i^{(p)}, x_j^{(q)})$ at scales p and q , the similarity score is computed as:

$$s(x_i^{(p)}, x_j^{(q)}) = \begin{cases} |p - q + 1|^{-\gamma_1} \cos(x_i^{(p)}, x_j^{(q)}), & \text{if } p > q; \\ |q - p + 1|^{-\gamma_2} \cos(x_i^{(p)}, x_j^{(q)}), & \text{if } p \leq q, \end{cases} \quad (16)$$

where γ_1 and γ_2 are non-negative hyperparameters that encourage feature diversity among experts. The causal similarity measure assigns higher similarity to positive pairs (coarser to finer scales), promoting alignment of samples with small scale gaps. For negative pairs (finer to coarser), it assigns higher similarity to push apart samples with larger scale gaps.

For expert k in our causal contrastive learning framework, consider the MMM output $z_{i,k}^p$ from sample $i \in \mathcal{B}_k$ at scale p . As mentioned previously, while outputs $z_{j,k}^p$ from other samples $j \in \mathcal{B}_k$ at

the same scale serve as natural positive candidates, the sample j has the risk of being routed incorrectly. To mitigate this, we augment the positive set with higher-scale representations ($q > p$) of the same sample. The negative set comprises both lower-scale representations and outputs from other experts. Formally, we define the positive and negative sets for $z_{i,k}^p$ as $\mathcal{P}_{i,k}^p$ and $\mathcal{N}_{i,k}^p$ respectively, yielding the following contrastive loss:

$$\mathcal{L}_C(k) = - \sum_{i \in \mathcal{B}_k} \sum_{p=1}^Q \frac{1}{|\mathcal{P}_{i,k}^p|} \sum_{z^* \in \mathcal{P}_{i,k}^p} \log \frac{\exp(s(z_{i,k}^{(p)}, z^*) \cdot \theta)}{\sum_{z' \in \mathcal{N}_{i,k}^p \cup \{z^*\}} \exp(s(z_{i,k}^{(p)}, z') \cdot \theta)}, \quad (17)$$

We use $\mathcal{L}_C(k)$ as an auxiliary objective to update the MMM layer and construct the final loss:

$$\mathcal{L} = \mathcal{L}_{\text{MAE}} + \lambda \sum_{l=1}^L \mathbb{E}_{k=1}^K (\mathcal{L}_C(k)), \quad (18)$$

where L denotes the number of backbone layers, and λ is a balancing hyperparameter.

Pattern Disentanglement for MMM. Each expert in MMM should focus on its respective temporal patterns, which essentially aim at achieving pattern disentanglement. Next, we explain in detail how $\mathcal{L}_C(k)$ achieves cross-expert pattern disentanglement, theoretically inspired by IP-IRM [42]. Assuming feature space \mathcal{X} is homogeneous under group G , any feature $x' \in \mathcal{X}$ can be transformed from $x \in \mathcal{X}$ via group action $g \cdot x$. We formally define the key concepts:

DEFINITION 1 (ORBIT AND PARTITION). *Given a subgroup $D \subset G$, it partitions the feature space \mathcal{X} into k disjoint subsets as $\mathcal{X} = \bigcup_{i=1}^k D(c_i \cdot x)$, where $\{c_i D\}_{i=1}^k$ are the cosets. These cosets form a factor group $G/D = \{c_i\}_{i=1}^k$. Here, each $c_i \cdot x$ serves as a representative feature for the i -th class, obtained through the group action on any feature $x \in \mathcal{X}$.*

MMM's top-1 routing strategy partitions input samples into k distinct classes, where G/D denotes transformations across experts, and D denotes transformations within an expert. We define a well-disentangled representation that can be separated into a *class-agnostic* component, which is invariant to G/D (cross-orbit) and equivariant to D (in-orbit), and a *class-specific* component, which is equivariant to G/D and invariant to D . We now prove that such disentanglement can be achieved via contrastive learning:

LEMMA 2. *The contrastive loss $-\log \frac{\exp(s(x_i, x_j))}{\sum_{x \in \mathcal{X}} \exp(s(x_i, x))}$ enforces the disentanglement of feature space \mathcal{X} for $(G/D) \times D$, where (x_i, x_j) are from the same orbit under group action D .*

The complete proof is provided in the Appendix B.2. This lemma establishes a theoretical connection between contrastive learning and disentangled representation learning. In the single-scale case, our contrastive loss $\mathcal{L}_C(k)$ simplifies to the conventional contrastive loss while still preserving cross-expert pattern disentanglement. The multiscale extension preserves this disentanglement while additionally emphasizing cross-scale differences, thereby enhancing MMM's multiscale processing capability.

5 Experiment

To evaluate the effectiveness of STM2/STM3, we answer the following five research questions:

- **RQ1:** How do our STM2/STM3 models perform on spatio-temporal time-series prediction tasks across diverse real-world domains, compared with existing baseline methods?
- **RQ2:** What are the individual contributions of each proposed module to the overall performance of the model?
- **RQ3:** How do different hyperparameter choices influence the predictive performance and stability of STM3?
- **RQ4:** How does the proposed Multiscale Mamba Module (MMM) effectively extract disentangled temporal patterns for each expert at each scale?
- **RQ5:** How does our proposed node-embedding-based routing strategy improve expert assignment smoothness and downstream prediction accuracy?

5.1 Experimental Setting

Datasets. To comprehensively evaluate the effectiveness of STM2/STM3, we select several real-world datasets spanning diverse application domains. These include three widely used transportation datasets, METR-LA [25], PEMS4, and PEMS8 [5], an air quality dataset KnowAir [41], a wireless traffic dataset Milan [3] (with three types of record), and a solar power dataset NREL [43]. These datasets have been extensively adopted in prior spatio-temporal time-series prediction research. Detailed descriptions of the datasets are provided in Appendix C.

Baselines and Metrics. Our STM2/STM3 model are evaluated on widely-used baselines for spatio-temporal time-series prediction, including RNN-based models (TGNN[52], MSDR[27]), CNN-based models (STGCN[48], STSGCN[39]), Attention-based models (ASTGCN[18], STAEformer[28], PromptST[51]), and Mamba-based models (SST[46], MixMamba[1], STGMamba[24]). We employed commonly used regression metrics, including Mean Absolute Error (MAE), Root Mean Squared Error (RMSE), and Mean Absolute Percentage Error (MAPE). More descriptions about the baselines are provided in Appendix C.

Implementation Details. The experiments are conducted on 4 Nvidia RTX3090 GPUs and implemented with PyTorch. We used the AdamW optimizer with an initial learning rate of $3e-3$. The batch size was 64, and the max training epochs were 100 for all models. The learning rate is halved after 25 epochs of training, and the early stop patience is 15 epochs. The dataset was split into training, validation, and testing parts with a 6:2:2 ratio. To evaluate STM2/STM3 under longer temporal settings than prior works [6, 24, 26, 36, 51], we set the input step $T = 48$ and the prediction horizon $\tau = 24$ for METR-LA, PEMS4, PEMS8, KnowAir, and NREL datasets. Due to the small size of the Milan dataset, we use $T = 12$ and $\tau = 12$ for it, which is also longer than the previous works' common setting [29–31, 47]. Each performance evaluation is repeated 5 times, and the average value is recorded.

5.2 Main Results (RQ1)

Table 1 demonstrates that STM2 and STM3 achieve state-of-the-art performance, ranking second-best and best, respectively, across all

Table 1: Performance comparison of STM2/STM3 and baselines. Bold denotes the best results and underline denotes the second-best results. “nan” denotes a failure to generate a valid output as a result of internal errors within the model.

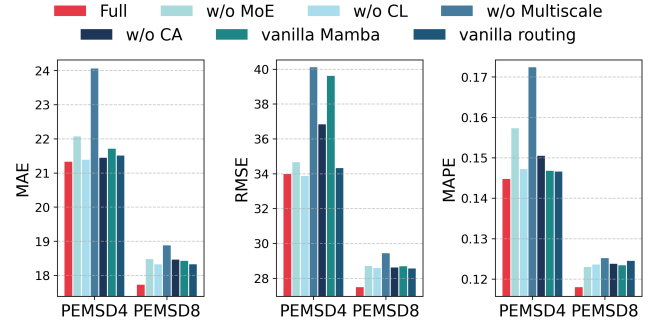
Model	METR-LA			PEMSD4			PEMSD8			KnowAir		
	MAE	RMSE	MAPE	MAE	RMSE	MAPE	MAE	RMSE	MAPE	MAE	RMSE	MAPE
STGCN	6.68	15.21	13.42	23.21	36.92	16.25	20.62	32.10	13.71	16.41	25.43	43.65
TGCN	6.82	15.44	16.31	30.17	47.68	21.17	22.51	36.31	15.01	16.48	26.07	43.32
ASTGCN	6.95	15.39	14.65	25.13	39.21	17.35	20.58	31.58	13.47	nan	nan	nan
STSGCN	6.58	15.28	15.55	27.36	42.56	19.16	22.06	34.22	15.11	16.75	26.31	44.31
MSDR	6.84	15.00	13.32	22.48	35.75	<u>15.52</u>	19.11	29.66	12.94	17.19	26.55	46.10
STAEformer	6.85	15.34	14.55	27.66	41.14	25.63	22.52	33.59	20.86	17.27	26.46	46.14
PromptST	6.40	15.13	14.54	28.41	43.25	20.65	24.03	36.48	16.01	17.04	26.31	45.31
SST	<u>6.93</u>	<u>15.46</u>	<u>16.15</u>	<u>33.03</u>	<u>52.74</u>	<u>22.71</u>	<u>24.00</u>	<u>39.85</u>	<u>15.51</u>	<u>16.92</u>	<u>26.65</u>	<u>43.85</u>
MixMamba	7.07	15.38	16.34	34.55	54.19	23.98	25.29	41.27	16.48	16.93	26.61	44.07
STGMamba	8.38	17.44	15.58	23.17	38.74	15.97	22.34	35.59	14.09	19.18	28.28	54.88
STM2	<u>6.13</u>	<u>14.58</u>	<u>12.39</u>	<u>22.08</u>	<u>34.68</u>	<u>15.74</u>	<u>18.49</u>	<u>28.72</u>	<u>12.31</u>	<u>16.01</u>	<u>25.21</u>	<u>42.22</u>
STM3	6.02	14.45	12.34	21.33	34.01	14.49	17.74	27.51	11.81	15.95	25.14	41.85

Model	Milan-SMS			Milan-Call			Milan-Internet			NREL		
	MAE	RMSE	MAPE	MAE	RMSE	MAPE	MAE	RMSE	MAPE	MAE	RMSE	MAPE
STGCN	14.52	37.96	42.64	11.88	34.04	43.56	72.35	208.44	29.79	2.77	4.83	16.85
TGCN	14.56	37.64	42.08	10.22	29.92	<u>36.82</u>	<u>57.61</u>	156.08	26.65	3.34	5.79	21.18
ASTGCN	14.38	36.13	42.35	11.72	31.46	41.53	72.68	188.31	37.73	2.97	5.07	18.67
STSGCN	29.64	53.93	85.42	24.15	45.55	79.31	136.74	251.46	123.20	3.36	5.68	20.76
MSDR	17.62	40.89	50.86	15.51	38.20	54.12	100.16	250.11	52.42	2.77	<u>4.75</u>	16.79
STAEformer	18.14	41.05	52.78	18.62	43.04	67.74	117.46	264.02	87.47	3.16	5.13	18.38
PromptST	18.41	44.07	51.47	16.65	43.53	55.66	76.30	194.09	33.08	3.54	5.61	22.43
SST	16.00	40.64	48.88	10.37	30.39	37.24	61.88	172.46	<u>26.14</u>	3.82	6.28	<u>23.03</u>
MixMamba	16.22	40.83	49.25	10.82	31.29	38.19	65.62	179.97	27.44	4.09	6.43	24.19
STGMamba	16.38	39.07	46.88	12.23	31.33	42.69	97.04	235.57	53.49	3.09	4.92	18.99
STM2	<u>13.40</u>	35.57	<u>38.12</u>	<u>10.19</u>	<u>26.95</u>	37.54	59.47	<u>150.46</u>	27.50	<u>2.66</u>	<u>4.75</u>	<u>16.52</u>
STM3	13.39	<u>35.97</u>	37.98	9.66	25.99	35.19	54.58	138.58	25.41	2.58	4.62	15.80

datasets. While RNN-based methods like MSDR show competitive results, their inability to capture multiscale patterns limits long-term forecasting. Pure time-series approaches (SST, MixMamba) underperform compared to spatio-temporal methods, underscoring the importance of spatio-temporal modeling. Notably, STG-Mamba’s strong performance on PEMS4 confirms Mamba’s capability for spatio-temporal modeling. STM2’s consistent improvements validate our multiscale fusion approach, and STM3’s additional gains demonstrate the MMM module’s effectiveness in enhancing multiscale feature extraction. Furthermore, the computational cost of models are compared in Appendix D.2.

5.3 Ablation Study (RQ2)

To validate STM3’s design, we conduct ablation studies on six variants: 1) **w/o MoE** (STM2): single Multiscale Mamba; 2) **w/o CL**: no contrastive learning; 3) **w/o Multiscale**: removes multiscale extraction; 4) **w/o CA**: no causal attention in AGCCN; 5) **vanilla Mamba**: replaces Multiscale Mamba with standard vanilla Mamba; 6) **vanilla routing**: input-based routing instead of node embeddings. Figure 3 shows that all components contribute significantly to performance. The multiscale mechanism has the largest impact,

**Figure 3: Ablation study of STM3.**

followed by MoE, aligned with our design principles. While individual contributions vary by dataset, each component proves essential for optimal spatio-temporal time-series prediction. More ablation study results are detailed in Appendix D.1

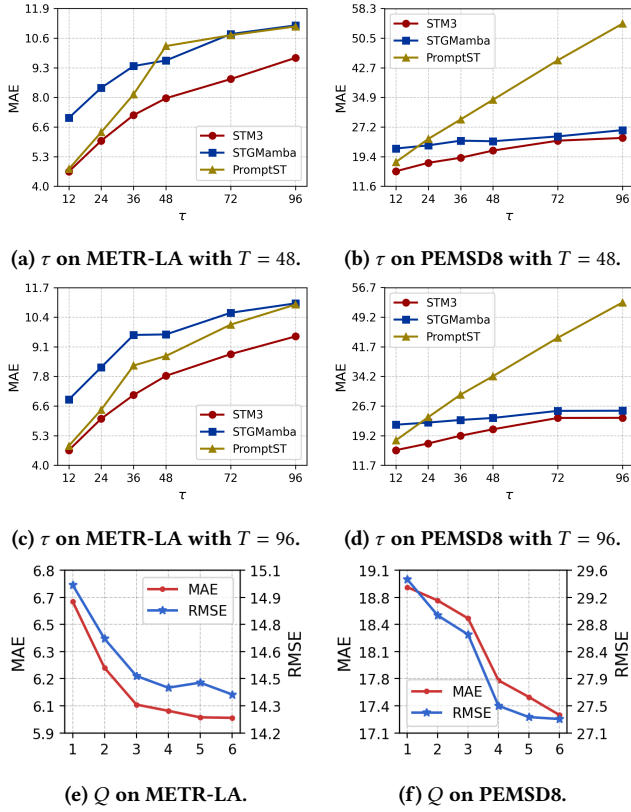


Figure 4: Hyperparameter Study.

5.4 Hyperparameter Study (RQ3)

As shown in Figure 4, we examine the effect of input step T , prediction horizon τ , and scale number Q on STM3's performance on METR-LA and PEMS8. To evaluate its long-term capability, we move beyond the commonly used short-term setting (typically $T = \tau = 12$ in prior works [6, 24, 26, 36, 51]) to $T = 48, 96$ and $\tau = 12 \sim 96$, comparing STM3 with the Mamba-based STGMamba and the Attention-based PromptST. Figures 4 (a)-(d) show that Mamba-based models maintain smoother performance curves, with STM3 consistently achieving SOTA results. We also vary Q from 1 to 6, finding initial gains followed by diminishing returns, which is shown in Figures 4 (e)-(f), indicating STM3's scale diversity is sufficient. Additional results are in Appendix D.3.

5.5 In-Depth Analysis (RQ4 & RQ5)

Expert-Wise Effectiveness. To validate MMM's expert-wise effectiveness to model complex spatio-temporal patterns, we visualized STM3's first-layer features using t-SNE [40]. Figure 5a shows distinct feature clusters for each expert, confirming effective pattern disentanglement. Figure 5b further illustrates the gating network's discriminative capability, with significantly varied assignment scores across experts for samples routed to the corresponding expert, indicating confident expert selection.

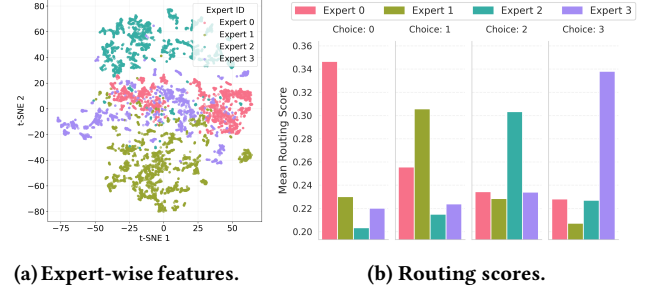


Figure 5: MMM's feature extraction across experts.

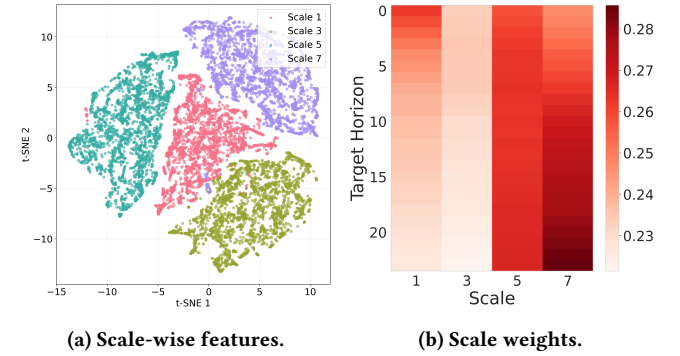


Figure 6: STM3's multiscale feature extraction.

Multiscale Feature Extraction. To evaluate STM3's multiscale extraction capability, we analyzed features from the first MMM expert by aggregating and visualizing scale-indexed features via t-SNE (Figure 6a). The results confirm that MMM experts successfully extract scale-specific features, validating our contrastive learning approach for scale-wise disentanglement. Moreover, we modified STM3 by inserting a learnable weighting parameter $\Gamma \in \mathbb{R}^{\tau \times Q}$ in the output layer, performing softmax-weighted scale fusion over scales for final predictions. As Figure 6b illustrates, Γ reveals an adaptive scale selection mechanism where larger scales become increasingly important for longer prediction horizons. This demonstrates STM3's capability to differentially process multiscale features based on temporal context.

Routing Strategy. To evaluate our node-embedding-based routing against traditional input-based routing, we compared their convergence patterns through expert assignment stability and loss trajectories. For the first test sample's MoE layer, we tracked epoch-wise expert assignments and computed inter-epoch "assignment changes" (nodes with altered allocations). Figure 7a shows our strategy achieves rapid convergence with minimal assignment fluctuations, while traditional routing exhibits persistent oscillations that persist even in later epochs. This observation confirms the better routing smoothness of our routing strategy. Similarly, Figure 7b demonstrates our approach's superior loss convergence with faster convergence values and lower final, confirming its performance advantage.

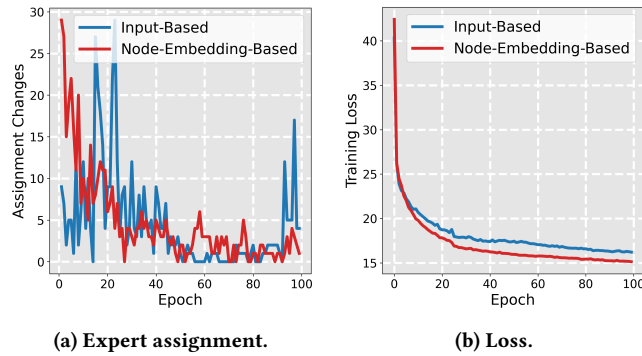


Figure 7: Comparison of routing strategies.

6 Conclusion

In this work, we propose STM2 for spatio-temporal time-series prediction, featuring: (1) a multiscale Mamba architecture to efficiently capture hierarchical information, and (2) an adaptive graph causal convolution network to model multiscale spatio-temporal dependencies. We further introduce STM3, an enhanced version employing a MoE architecture with a stable routing strategy and causal contrastive learning to improve scale distinguishability. Theoretical analysis and experiments demonstrate that STM3 achieves superior routing smoothness and ensures effective pattern disentanglement per expert. This work advances MoE in spatio-temporal time-series prediction, offering insights into multilevel information fusion and inspiring future model development.

Acknowledgments

To Robert, for the bagels and explaining CMYK and color spaces.

References

- [1] Khaled Alkilani, Yihang He, and Der-Horng Lee. 2024. MixMamba: Time series modeling with adaptive expertise. *Information Fusion* 112 (2024), 102589.
- [2] Lei Bai, Lina Yao, Can Li, Xianzhi Wang, and Can Wang. 2020. Adaptive graph convolutional recurrent network for traffic forecasting. *Advances in neural information processing systems* 33 (2020), 17804–17815.
- [3] Gianni Barlacchi, Marco De Nadai, Roberto Larcher, Antonio Casella, Cristiana Chitic, Giovanni Torrisi, Fabrizio Antonelli, Alessandro Vespignani, Alex Pentland, and Bruno Lepri. 2015. A multi-source dataset of urban life in the city of Milan and the Province of Trentino. *Scientific data* 2, 1 (2015), 1–15.
- [4] Xiuding Cai, Yaoyao Zhu, Xueyao Wang, and Yu Yao. 2024. MambaTS: improved selective state space models for long-term time series forecasting. *arXiv preprint arXiv:2405.16440* (2024).
- [5] Chao Chen, Karl Petty, Alexander Skabardonis, Pravin Varaiya, and Zhanfeng Jia. 2001. Freeway performance measurement system: mining loop detector data. *Transportation research record* 1748, 1 (2001), 96–102.
- [6] Min Chen, Guansong Pang, Wenjun Wang, and Cheng Yan. 2025. Information Bottleneck-guided MLPs for Robust Spatial-temporal Forecasting. In *Forty-second International Conference on Machine Learning*.
- [7] Peng Chen, Yingying ZHANG, Yunyao Cheng, Yang Shu, Yihang Wang, Qingsong Wen, Bin Yang, and Chenjuan Guo. 2023. Pathformer: Multi-scale Transformers with Adaptive Pathways for Time Series Forecasting. In *The Twelfth International Conference on Learning Representations*.
- [8] Zixiang Chen, Yihe Deng, Yue Wu, Quanquan Gu, and Yuanzhi Li. 2022. Towards understanding mixture of experts in deep learning. *arXiv preprint arXiv:2208.02813* (2022).
- [9] Jeongwhan Choi, Hwangyong Choi, Jeehyun Hwang, and Noseong Park. 2022. Graph neural controlled differential equations for traffic forecasting. In *Proceedings of the AAAI conference on artificial intelligence*, Vol. 36. 6367–6374.
- [10] Jinhyeok Choi, Heehyeon Kim, Minhyeong An, and Joyce Jiyoung Whang. 2024. Spot-mamba: Learning long-range dependency on spatio-temporal graphs with selective state spaces. *arXiv preprint arXiv:2406.11244* (2024).
- [11] Damai Dai, Chengqi Deng, Chenggang Zhao, Rx Xu, Huazuo Gao, Deli Chen, Jiashi Li, Wangding Zeng, Xingkai Yu, Y Wu, et al. 2024. DeepSeekMoE: Towards Ultimate Expert Specialization in Mixture-of-Experts Language Models. In *Proceedings of the 62nd Annual Meeting of the Association for Computational Linguistics (Volume 1: Long Papers)*. 1280–1297.
- [12] Tri Dao, Daniel Y Fu, Khaled K Saab, Armin W Thomas, Atri Rudra, and Christopher Ré. 2023. Hungry Hungry Hippos: Towards Language Modeling with State Space Models. In *Proceedings of the 11th International Conference on Learning Representations (ICLR)*.
- [13] Nan Du, Yanping Huang, Andrew M Dai, Simon Tong, Dmitry Lepikhin, Yuanzhong Xu, Maxim Krikun, Yanqi Zhou, Adams Wei Yu, Orhan Firat, et al. 2022. Glam: Efficient scaling of language models with mixture-of-experts. In *International conference on machine learning*. PMLR, 5547–5569.
- [14] Yuchen Fang, Yanjun Qin, Haiyong Luo, Fang Zhao, Bingbing Xu, Liang Zeng, and Chenxing Wang. 2023. When spatio-temporal meet wavelets: Disentangled traffic forecasting via efficient spectral graph attention networks. In *2023 IEEE 39th international conference on data engineering (ICDE)*. IEEE, 517–529.
- [15] William Fedus, Barret Zoph, and Noam Shazeer. 2022. Switch transformers: Scaling to trillion parameter models with simple and efficient sparsity. *Journal of Machine Learning Research* 23, 120 (2022), 1–39.
- [16] Albert Gu and Tri Dao. 2024. Mamba: Linear-Time Sequence Modeling with Selective State Spaces. In *First Conference on Language Modeling*.
- [17] Albert Gu, Karan Goel, and Christopher Ré. 2021. Efficiently modeling long sequences with structured state spaces. *arXiv preprint arXiv:2111.00396* (2021).
- [18] Shengnan Guo, Youfang Lin, Ning Feng, Chao Song, and Huaiyu Wan. 2019. Attention based spatial-temporal graph convolutional networks for traffic flow forecasting. In *Proceedings of the AAAI conference on artificial intelligence*, Vol. 33. 922–929.
- [19] Robert A Jacobs, Michael I Jordan, Steven J Nowlan, and Geoffrey E Hinton. 1991. Adaptive mixtures of local experts. *Neural computation* 3, 1 (1991), 79–87.
- [20] Albert Q Jiang, Alexandre Sablayrolles, Antoine Roux, Arthur Mensch, Blanche Savary, Chris Bamford, Devendra Singh Chaplot, Diego de las Casas, Emma Bou Hanna, Florian Bressand, et al. 2024. Mixtral of experts. *arXiv preprint arXiv:2401.04088* (2024).
- [21] Dmitry Lepikhin, Hyoungho Lee, Yuanzhong Xu, Dehao Chen, Orhan Firat, Yanping Huang, Maxim Krikun, Noam Shazeer, and Zhifeng Chen. 2020. Gshard: Scaling giant models with conditional computation and automatic sharding. *arXiv preprint arXiv:2006.16668* (2020).
- [22] Dongyuan Li, Shiyin Tan, Ying Zhang, Ming Jin, Shirui Pan, Manabu Okumura, and Renhe Jiang. 2024. Dyg-mamba: Continuous state space modeling on dynamic graphs. *arXiv preprint arXiv:2408.06966* (2024).
- [23] Hongbo Li, Sen Lin, Lingjie Duan, Yingbin Liang, and Ness B Shroff. 2024. Theory on mixture-of-experts in continual learning. *arXiv preprint arXiv:2406.16437* (2024).
- [24] Lincan Li, Hanchen Wang, Wenjie Zhang, and Adelle Coster. 2024. Stg-mamba: Spatial-temporal graph learning via selective state space model. *arXiv preprint arXiv:2403.12418* (2024).
- [25] Yaguang Li, Rose Yu, Cyrus Shahabi, and Yan Liu. 2018. Diffusion Convolutional Recurrent Neural Network: Data-Driven Traffic Forecasting. In *International Conference on Learning Representations*.
- [26] Zhonghang Li, Lianghao Xia, Yong Xu, and Chao Huang. 2023. GPT-ST: generative pre-training of spatio-temporal graph neural networks. *Advances in neural information processing systems* 36 (2023), 70229–70246.
- [27] Dachuan Liu, Jin Wang, Shuo Shang, and Peng Han. 2022. Msdr: Multi-step dependency relation networks for spatial temporal forecasting. In *Proceedings of the 28th ACM SIGKDD conference on knowledge discovery and data mining*. 1042–1050.
- [28] Hangchen Liu, Zheng Dong, Renhe Jiang, Jiewen Deng, Jinliang Deng, Quan-jun Chen, and Xuan Song. 2023. Spatio-temporal adaptive embedding makes vanilla transformer sota for traffic forecasting. In *Proceedings of the 32nd ACM international conference on information and knowledge management*. 4125–4129.
- [29] Shang Liu, Miao He, Zhiqiang Wu, Peng Lu, and Weixi Gu. 2024. Spatial-temporal graph neural network traffic prediction based load balancing with reinforcement learning in cellular networks. *Information Fusion* 103 (2024), 102079.
- [30] Ali Mehrabian, Shahab Bahrami, and Vincent WS Wong. 2023. A dynamic Bernstein graph recurrent network for wireless cellular traffic prediction. In *ICC 2023-IEEE International Conference on Communications*. IEEE, 3842–3847.
- [31] Ali Mehrabian and Vincent WS Wong. 2025. A-Gamba: An Adaptive Graph-Mamba Model for Traffic Prediction in Wireless Cellular Networks. *IEEE Wireless Communications Letters* (2025).
- [32] Harsh Mehta, Ankit Gupta, Ashok Cutkosky, and Behnam Neyshabur. 2023. Long Range Language Modeling via Gated State Spaces. In *International Conference on Learning Representations*.
- [33] Huy Nguyen, Pedram Akbarian, Fanqi Yan, and Nhat Ho. 2023. Statistical perspective of top-k sparse softmax gating mixture of experts. *arXiv preprint arXiv:2309.13850* (2023).
- [34] Huy Nguyen, Nhat Ho, and Alessandro Rinaldo. 2024. On least square estimation in softmax gating mixture of experts. *arXiv preprint arXiv:2402.02952* (2024).

- [35] Mohammad Amin Shabani, Amir H Abdi, Lili Meng, and Tristan Sylvain. [n.d.]. Scaleformer: Iterative Multi-scale Refining Transformers for Time Series Forecasting. In *The Eleventh International Conference on Learning Representations*.
- [36] Zhi Sheng, Yuan Yuan, Jingtao Ding, and Yong Li. 2025. Unveiling the Power of Noise Priors: Enhancing Diffusion Models for Mobile Traffic Prediction. *arXiv preprint arXiv:2501.13794* (2025).
- [37] Xiaoming Shi, Shiyu Wang, Yuqi Nie, Dianqi Li, Zhou Ye, Qingsong Wen, and Ming Jin. 2024. Time-MoE: Billion-Scale Time Series Foundation Models with Mixture of Experts. *arXiv preprint arXiv:2409.16040* (2024).
- [38] Jimmy TH Smith, Andrew Warrington, and Scott W Linderman. 2023. Simplified State Space Layers for Sequence Modeling. In *ICLR*.
- [39] Chao Song, Youfang Lin, Shengnan Guo, and Huaiyu Wan. 2020. Spatial-temporal synchronous graph convolutional networks: A new framework for spatial-temporal network data forecasting. In *Proceedings of the AAAI conference on artificial intelligence*, Vol. 34. 914–921.
- [40] Laurens Van der Maaten and Geoffrey Hinton. 2008. Visualizing data using t-SNE. *Journal of machine learning research* 9, 11 (2008).
- [41] Shuo Wang, Yanran Li, Jiang Zhang, Qingye Meng, Lingwei Meng, and Fei Gao. 2020. Pm2.5-gnn: A domain knowledge enhanced graph neural network for pm2.5 forecasting. In *Proceedings of the 28th international conference on advances in geographic information systems*. 163–166.
- [42] Tan Wang, Zhongqi Yue, Jianqiang Huang, Qianru Sun, and Hanwang Zhang. 2021. Self-supervised learning disentangled group representation as feature. *Advances in Neural Information Processing Systems* 34 (2021), 18225–18240.
- [43] Yuankai Wu, Dingyi Zhuang, Aurelie Labbe, and Lijun Sun. 2021. Inductive graph neural networks for spatiotemporal kriging. In *Proceedings of the AAAI conference on artificial intelligence*, Vol. 35. 4478–4485.
- [44] Zonghan Wu, Shirui Pan, Guodong Long, Jing Jiang, Xiaojun Chang, and Chengqi Zhang. 2020. Connecting the dots: Multivariate time series forecasting with graph neural networks. In *Proceedings of the 26th ACM SIGKDD international conference on knowledge discovery & data mining*. 753–763.
- [45] Zonghan Wu, Shirui Pan, Guodong Long, Jing Jiang, and Chengqi Zhang. 2019. Graph wavenet for deep spatial-temporal graph modeling. *arXiv preprint arXiv:1906.00121* (2019).
- [46] Xiongqiao Xu, Canyu Chen, Yueqing Liang, Baixiang Huang, Guangji Bai, Liang Zhao, and Kai Shu. 2024. SST: Multi-Scale Hybrid Mamba-Transformer Experts for Long-Short Range Time Series Forecasting. *arXiv preprint arXiv:2404.14757* (2024).
- [47] Yang Yao, Bo Gu, Zhou Su, and Mohsen Guizani. 2021. MVSTGN: A multi-view spatial-temporal graph network for cellular traffic prediction. *IEEE Transactions on Mobile Computing* 22, 5 (2021), 2837–2849.
- [48] Bing Yu, Haoteng Yin, and Zhanxing Zhu. 2017. Spatio-temporal graph convolutional networks: A deep learning framework for traffic forecasting. *arXiv preprint arXiv:1709.04875* (2017).
- [49] Haonan Yuan, Qingyun Sun, Zhaonan Wang, Xingcheng Fu, Cheng Ji, Yongjian Wang, Bo Jin, and Jianxin Li. 2025. DG-Mamba: Robust and Efficient Dynamic Graph Structure Learning with Selective State Space Models. In *Proceedings of the AAAI Conference on Artificial Intelligence*, Vol. 39. 22272–22280.
- [50] Zijian Zhang, Ze Huang, Zhiwei Hu, Xiangyu Zhao, Wanyu Wang, Zitao Liu, Junbo Zhang, S Joe Qin, and Hongwei Zhao. 2023. Mlpst: Mlp is all you need for spatio-temporal prediction. In *Proceedings of the 32nd ACM International Conference on Information and Knowledge Management*. 3381–3390.
- [51] Zijian Zhang, Xiangyu Zhao, Qidong Liu, Chunxu Zhang, Qian Ma, Wanyu Wang, Hongwei Zhao, Yiqi Wang, and Zitao Liu. 2023. Promptst: Prompt-enhanced spatio-temporal multi-attribute prediction. In *Proceedings of the 32nd ACM International Conference on Information and Knowledge Management*. 3195–3205.
- [52] Ling Zhao, Yujiao Song, Chao Zhang, Yu Liu, Pu Wang, Tao Lin, Min Deng, and Haifeng Li. 2019. T-GCN: A temporal graph convolutional network for traffic prediction. *IEEE transactions on intelligent transportation systems* 21, 9 (2019), 3848–3858.
- [53] Barret Zoph. 2022. Designing effective sparse expert models. In *2022 IEEE International Parallel and Distributed Processing Symposium Workshops (IPDPSW)*. IEEE, 1044–1044.

A More Related Work

State Space Models. SSMs have demonstrated exceptional capability in modeling sequential dependencies via state space. The structured state-space sequence model (S4) [17] pioneered efficient long-range dependency modeling with linear complexity. Subsequent advancements led to variants such as S5 [38], H3 [12], and

GSS [32]. Mamba [16] marked a breakthrough by introducing data-dependent SSM parameters and parallel scan selection (S6), surpassing quadratic-complexity transformers in processing long sequences while maintaining linear computational efficiency. In the domain of spatio-temporal and time-series modeling, Mamba has emerged as a powerful component [1, 4, 10, 24, 46]. For instance, SST [46] employs hybrid Mamba-Transformer experts to model long- and short-range time series patterns, adaptively balancing the contributions of the two experts via a long-short router to integrate global trends and local variations. MixMamba [1] utilizes multiple Mamba layers as experts, incorporating MoE mechanism to effectively model heterogeneous and non-stationary time series data. STG-Mamba [24] combines GNNs with selective SSMs, dynamically updating adjacency matrices through Kalman filter-based graph neural networks. Spot-Mamba [10] generates node embeddings by scanning node-specific walk sequences and performing temporal scans to capture long-range spatio-temporal dependencies. In our work, we further identify and exploit the connection between different scales, deriving a novel multiscale Mamba architecture for spatio-temporal dependency modeling.

Mixture-of-Experts. The MoE is a classical neural network architecture [19] designed to increase model capacity with minimal computational overhead. Recently, MoE networks have become integral components in deep neural networks, notably in large language models, achieving remarkable success [11, 13, 15, 20, 21, 53]. By employing a gating network to route different data subsets to a small group of expert networks with identical architectures, MoE enables specialized experts to effectively model distinct data patterns, thus enhancing overall model capacity. Recent theoretical studies have further analyzed the superior performance of MoE structures, elucidating their inherent advantages [8, 23, 33, 34]. In the time-series modeling domain, several studies have leveraged MoE’s capabilities to handle complex data distributions [1, 37, 46]. In this work, we propose a novel routing strategy based on node embeddings, which enforces each routed expert to capture data distributions at the granularity of spatial nodes. By utilizing our proposed multiscale Mamba as experts, our model demonstrates strong fitting capabilities for complex multiscale patterns.

B Proof

B.1 Proof of Lemma 1

We proceed with three steps:

1. **Pairwise Bound:** Each pairwise disagreement is bounded as:

$$p_{i,j} \leq \rho K^2 \|\mathbf{h}_i - \mathbf{h}_j\|_\infty \quad (19)$$

Given random variable $\{r_k\}_{k=1}^K$, let $k_1 = \operatorname{argmax}_{m \in [K]} \{h_{i,k} + r_k\}$ and

$k_2 = \operatorname{argmax}_{k \in [K]} \{h_{j,k} + r_k\}$, then we have that

$$h_{i,k_1} + r_{k_1} > h_{i,k_2} + r_{k_2}, \quad h_{j,k_1} + r_{k_1} > h_{j,k_2} + r_{k_2}, \quad (20)$$

which implies that

$$h_{j,k_2} - h_{j,k_1} > r_{k_1} - r_{k_2} > h_{i,k_2} - h_{i,k_1}. \quad (21)$$

Define $C(k_1, k_2) = \frac{h_{j,k_2} - h_{j,k_1} + h_{i,k_2} - h_{i,k_1}}{2}$, then (21) implies that:

$$|r_{k_1} - r_{k_2} - C(k_1, k_2)| \leq \frac{|h_{j,k_2} - h_{j,k_1} - h_{i,k_2} + h_{i,k_1}|}{2} \leq \|\mathbf{h}_i - \mathbf{h}_j\|_\infty \quad (22)$$

For any $i, j \in [M]$, the pairwise disagreement probability is bounded as:

$$\begin{aligned} p_{i,j} &= \mathbb{P} \left(\underset{k \in [K]}{\operatorname{argmax}} \{h_{i,k} + r_k\} \neq \underset{k \in [K]}{\operatorname{argmax}} \{h_{j,k} + r_k\} \right) \\ &\leq \mathbb{P} (\exists k_1 \neq k_2 \in [K], \text{ s.t. } |r_{k_1} - r_{k_2} - C(k_1, k_2)| \leq \|\mathbf{h}_i - \mathbf{h}_j\|_\infty) \\ &\leq \sum_{k_1 < k_2} \mathbb{P} (|r_{k_1} - r_{k_2} - C(k_1, k_2)| \leq \|\mathbf{h}_i - \mathbf{h}_j\|_\infty) \\ &= \sum_{k_1 < k_2} \mathbb{E} [r_{k_2} + C(k_1, k_2) - \|\mathbf{h}_i - \mathbf{h}_j\|_\infty \leq r_{k_1} \\ &\quad \leq r_{k_2} + C(k_1, k_2) + \|\mathbf{h}_i - \mathbf{h}_j\|_\infty] \\ &\leq \sum_{k_1 < k_2} 2\rho \|\mathbf{h}_i - \mathbf{h}_j\|_\infty \\ &\leq \rho K^2 \|\mathbf{h}_i - \mathbf{h}_j\|_\infty, \end{aligned}$$

2. Upper Bound:

$$\begin{aligned} P &= \mathbb{P} \left(\exists i \neq j \in [M], \text{ s.t. } \underset{k \in [K]}{\operatorname{argmax}} \{h_{i,k} + r_k\} \neq \underset{k \in [K]}{\operatorname{argmax}} \{h_{j,k} + r_k\} \right) \\ &\leq \sum_{i < j} \mathbb{P} \left(\underset{k \in [K]}{\operatorname{argmax}} \{h_{i,k} + r_k\} \neq \underset{k \in [K]}{\operatorname{argmax}} \{h_{j,k} + r_k\} \right) \\ &\leq \sum_{i < j} p_{i,j} \\ &\leq \rho K^2 \sum_{i < j} \|\mathbf{h}_i - \mathbf{h}_j\|_\infty, \end{aligned}$$

3. Lower Bound: When all \mathbf{h}_i are identical, $\|\mathbf{h}_i - \mathbf{h}_j\|_\infty = 0$ and the probability equals 0. This condition is met for our routing strategy, since the gating output \mathbf{h}_i of every sample is generated by the same node embedding E_A . Obviously, for the traditional input-based routing strategy, such a condition cannot be achieved, since it means all input time series are the same.

B.2 Proof of Lemma 2

Consider the contrastive loss

$$\mathcal{L}_{\text{contr}} = -\log \frac{\exp(s(x_i, x_j))}{\sum_{x \in \mathcal{X}} \exp(s(x_i, x))},$$

where $x_i = \phi(I_i)$ and $x_j = \phi(I_j)$ are features extracted from two inputs I_i and I_j belonging to the same orbit under the subgroup $D \subset G$. The loss encourages the similarity between x_i and x_j by maximizing the similarity $s(x_i, x_j)$ while simultaneously minimizing the similarity to all other features in the denominator. Since $I_j = d \cdot I_i$ for some $d \in D$, this enforces that the expert ϕ must produce features that are equivariant under D -actions; otherwise, $s(x_i, x_j)$ would be suboptimal, increasing the loss. Therefore, minimizing $\mathcal{L}_{\text{contr}}$ enforces that $\phi(d \cdot I) = d \cdot \phi(I)$ for all $d \in D$, leading to D -equivariance in the representation space \mathcal{X} .

Simultaneously, for negative samples $x_k = \phi(I_k)$ where I_k belongs to a different orbit under D —specifically, $I_k = c \cdot I_i$ for some

$c \in G/D$ —the loss penalizes the similarity $\exp(x_i^\top x_k)$. This encourages the model to minimize any alignment between x_i and features from other orbits, thus pushing the representation ϕ to become invariant under the action of G/D . In other words, $\phi(c \cdot I) = \phi(I)$ must hold for all $c \in G/D$ to effectively suppress cross-orbit similarity in the contrastive objective.

Combining the above, we conclude that the learned feature space \mathcal{X} admits a decomposition of the form

$$\mathcal{X} = \mathcal{X}_{G/D} \times \mathcal{X}_D,$$

where $\mathcal{X}_{G/D}$ is invariant to D -actions and sensitive to G/D , while \mathcal{X}_D is equivariant to D -actions and invariant to G/D . To verify this decomposition formally, let $g = (c, d) \in G = (G/D) \times D$. Then for any $x = \phi(I)$,

$$g \cdot x = \phi(g \cdot I) = \phi(c \cdot (d \cdot I)) = \phi(d \cdot I) = d \cdot \phi(I) = d \cdot x,$$

where the third equality follows from G/D -invariance and the fourth from D -equivariance. This confirms that the group action affects only the D -equivariant component \mathcal{X}_D , while the G/D -invariant component remains unaffected. Hence, the contrastive loss induces a disentangled representation aligned with the product structure of the group G , satisfying the desired properties of equivariance and decomposability.

C Implementation Details

Data. Several large-scale real-world experiments were selected to evaluate the effectiveness of STM2/STM3. The METR-LA dataset comprises traffic statistics collected from the road network of Los Angeles County, reflecting daily spatio-temporal patterns [25]. Meanwhile, the PEMS4 and PEMS8 datasets are part of the Caltrans Performance Measurement System [5]. The KnowAir dataset records the PM2.5 of several regions in China [41]. The real-world wireless traffic dataset collected by Telecom Italia in Milan [3]. The dataset comprises three types of cellular services: SMS, voice calls, and Internet usage. For our experiments, we randomly select 300 cells from a total of 10,000 across the city. The NREL dataset registered solar power output by photovoltaic power plants in Alabama [43]. These datasets are widely adopted in prior research. Detailed statistical descriptions are provided in Table 2.

Baselines. Our STM2/STM3 model is evaluated on a set of widely-used baselines for spatio-temporal time-series prediction as follows:

- **STGCN**[48] extracts spatio-temporal features by GCN and CNN.
- **TGCN**[52] extracts spatio-temporal features by GNN and RNN.
- **STSGCN**[39] constructs a local spatio-temporal graph to model spatio-temporal correlation.
- **MSDR**[27] uses RNN to capture long-term temporal information and uses GNN to model the spatio-temporal correlations.
- **ASTGCN**[18] uses an attention mechanism and GNN to model spatio-temporal information.
- **STAEformer**[28] generated an adaptive graph by learnable node embeddings to model spatial dependency and uses Transformer to model temporal dependency.

Table 2: Statistical Information of Experimental Dataset

Dataset	Data Record	Node	Sample Rate	Time Range
METR-LA	transport traffic speed	207	5-minute	2012.03 - 2012.06
PEMS04	transport traffic volume	307	5-minute	2018.01 - 2018.02
PEMS08	transport traffic volume	170	5-minute	2016.07 - 2016.08
KnowAir	air quality	184	3-hour	2015.01 - 2018.12
Milan	mobile traffic volume	300	1-hour	2013.11 - 2014.01
NREL	solar power output	137	10-minute	2006.01 - 2006.03

- **PromptST**[51] dynamically generates task-specific prompts to capture spatio-temporal dependency.
- **SST**[46] using hybrid Mamba and Transformer experts to model temporal dependency.
- **MixMamba**[1] uses several Mamba layers as experts, incorporating an MoE mechanism to model the heterogeneous and non-stationary time series data.
- **STGMamba**[24] uses Kalman filtering GNN to model spatial dependency and uses Mamba to model temporal dependency.

D Additional Experiments

D.1 More Ablation Study

In this section, we provide more results of the ablation study of STM3 in Figure 8.

D.2 Computation Cost

In this section, we compare the computation efficiency of STM2/STM3 with other baselines on the PEMS08 dataset in terms of training time, testing time, training memory, and testing memory. The computation cost of testing demonstrates the efficiency of the inference phase. The peak memory usage was recorded by torch method “torch.cuda.max_memory_allocated()”. For all models, the batch

size is set to 64. The results are summarized in Table 3. We observe that STM3’s training cost is high, but the inference cost is low. This is the result of both contrastive learning in the training phase and MoE’s mechanism.

D.3 Hyperparameter Sensitivity Analysis

We varied the dimension of the feature of each spatio-temporal step d , the dimension of the feature of each spatial node d_e , the number of routed experts K , the input step length T , the prediction horizon length τ , and the number of scales Q (if $Q = i$, means that the scale list of STM3 is $S = [1, 3, 5, \dots, 2i - 1]$). The results are summarized in Figure 9.

E Limitations and future directions

The datasets used by this work do not cover all spatio-temporal datasets. We will explore using larger dataset collections to further improve STM3.

STM3 gives a new idea for spatio-temporal modeling, particularly in scenarios requiring fine-grained, long-term predictions. We plan to build a foundation model using multiple spatio-temporal datasets using STM3’s framework to further explore its scalability.

Received 20 February 2007; revised 12 March 2009; accepted 5 June 2009

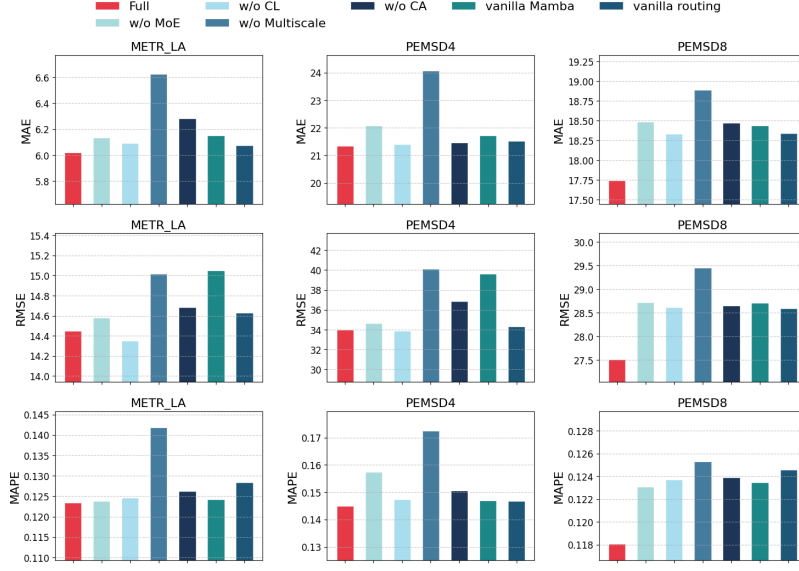


Figure 8: Ablation study of STM3.

Table 3: The computation cost on PEMS8 dataset.

Models	Computation Time		Memory	
	Training (s/epoch)	Testing (s/epoch)	Training (GB)	Testing (GB)
STGCN	23.07	2.53	3.77	1.74
MSDR	94.94	12.00	6.10	0.68
ASTGCN	54.22	8.49	3.25	1.13
STAEformer	77.60	11.31	16.88	3.43
SST	33.44	4.34	2.20	0.88
MixMamba	122.14	10.82	4.96	1.49
STGMamba	47.64	3.30	1.26	0.70
STM2	34.71	3.13	2.60	0.76
STM3	82.43	5.99	13.09	0.80

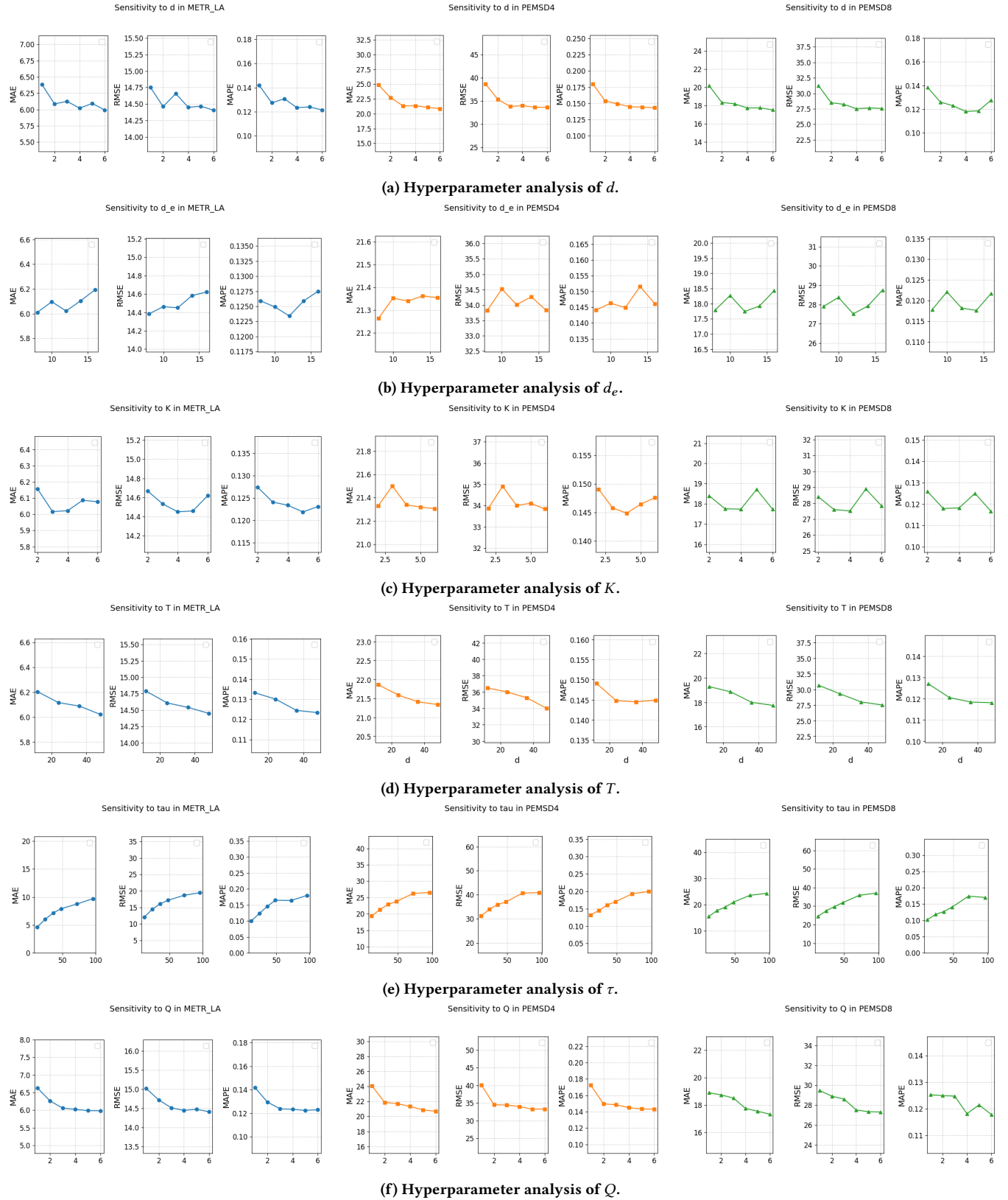


Figure 9: Hyperparameter analysis of STM3.